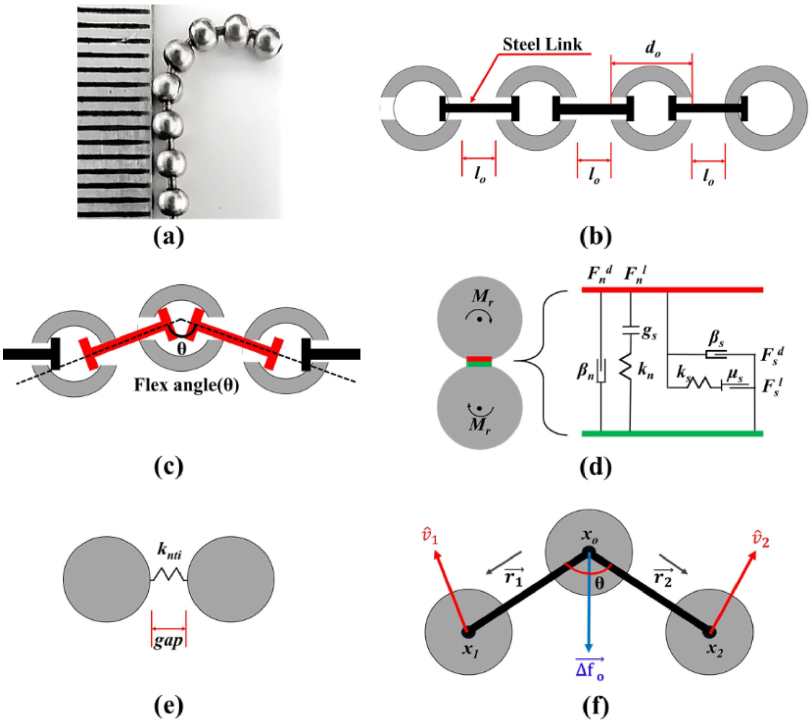

Fig. S6. Geometric characteristics of the flexible granular chains (a) Photograph of the metallic flexible granular chain modelled in this study. (b) I-shaped links with a maximum elongation length of l_0 connecting two beads in the chain, wherein their geometry constraints the elongation between two spherical steel beads to remain less or equal to l_0. (c) Angular constraint on two consecutive links in the chain, due to their geometry, the links lock in the cavity whenever the bending angle between two consecutive links becomes less or equal to the flex angle θ_0 (d) Contact created by the overlap of two particles shown in the red-green bar with the rolling moment acting on the contacting particles at their centres and the expanded linear contact shows the behaviour and rheological components of linear contact model implemented at frictional contacts. (e) DEM implementation of the elongation constraint in the flexible granular chain, wherein the k_{nti} is the linear elastic stiffness, and its value is assumed to be a function of the gap between the two spheres. (f) Angular constraint implementation in DEM contact model for flexible granular chains, the forces are applied along the directions of $\hat{v}_1$, $\hat{v}_2$ and $\hat{v}_3$ vectors such that the linear and the angular momentum of the system is conserved.

5. DEM contact model

The flexible granular chains simulated in this study are composed of metallic beads connected by I-shaped links (Fig.S6a,b). . The flanges of the connecting links are locked inside a cavity within the beads (Fig.S6b). The average diameter of the beads is $d_0 = 2$mm, and the chain length (N) is described by the number of beads or monomers in the chain. One simple measure of the flexibility of these chains is the diameter of the smallest possible closed-loop it can form. The chains simulated in this study have a characteristic closed-loop diameter of ∼8 mm, and this is independent of the number of monomers for the chains with N > 4. The I-shaped link connectors between the beads impose constraints on the kinematics and the range of attainable geometric configurations for these chains, dictating both their micro and macro-level behaviour.

In our study, we decouple the effect of the link connectors into two superimposed kinematic constraints on the motion of beads, i.e. the elongation constraint and the angular constraint. The elongation constraint arises from the shape of the link, wherein the gap between two connected beads can extend up to a maximum elongation of l_0 without any significant tensile forces being generated in the link, but after the elongation exceeds l_0, the links lock and become practically rigid for any further elongation, and this constraint remains valid for the range of forces experienced in the angle of repose experiments. The chains used in this study have $l_0 = 1$mm (Fig.S6b). The geometry of the links also imposes an angular constraint on the bending angle between two consecutive links connecting three continuous beads in a chain (Fig.S6c). This bending angle θ is constrained to remain greater or equal to a characteristic bending angle called the flex angle denoted by θ_0. If the bending angle is greater or equal to the flex angle θ_0, two consecutive links can bend freely but become practically rigid for bending angles smaller than the flex angle. For the chains simulated in this study, this characteristic flex angle $\theta_0 = 140°$. Unlike the angular constraint, the link geometry does not constrain the twisting of the beads along the axis of their inner cavity.

In this study, we use the DEM software PFC3D for the simulations, wherein the steel beads in the chains are idealized as freely rotating rigid and perfectly spherical particles, having a diameter of $d_0 = 2$mm. Whenever two particles, which are not connected by a link, come in contact with each other, they overlap, and the distance between the centres of two particles becomes smaller than the average diameter of the contacting particles, they form a frictional contact (Fig.S6d). We employ a linear elastic contact model at the frictional contacts (Fig.S6d) wherein the incremental forces and moments applied to the contacting particles are calculated from their relative incremental displacement and velocities by the equations 9 to 14:

$$\delta F_n = \delta F_n^l + \delta F_n^d \quad [9]$$

$$\delta F_n = k_n \delta n - 2\beta_n (m * k_n)^{0.5} \delta \dot{n} \quad [10]$$

$$\delta F_s = k_s \delta s - 2\beta_s (m * k_s)^{0.5} \delta \dot{s} \quad [11]$$

$$F_s <= \mu_s F_n \quad [12]$$

$$\delta M_r = -k_s \frac{d_0}{2} \delta\theta \quad [13]$$

$$M_r <= \mu_r \frac{d_0}{2} F_n \quad [14]$$

Where δF_n and δF_s are the incremental normal and tangential forces acting on the contacting particles, δF^l and δF^d are linear elastic and damping components of the force increments, k_n and k_t are the normal and tangential stiffness of the contact, δn and δs are the relative normal and tangential displacement increments at the contact. β_n and β_s are the viscous damping coefficient in the normal and tangential direction and are implemented to prevent the persistence of vibrations in the system. μ_s and μ_r are the sliding and rolling friction coefficients at the contact, with sliding Coulomb friction capping the magnitude of the tangential linear force acting at the contact. $\delta\theta$ is the relative incremental rotation of the particles relative to the contact point. Finally, m and d_0 are the average mass and diameter of the particles at the contact. For perfectly spherical particles in DEM simulations, the rolling frictional component is necessary to capture the rolling resistance observed in industry-manufactured spherical granular particles with inherent shape imperfections. Rolling resistance moment M_r acts in the direction opposite to that of the rotational increment $\delta\theta$, and its magnitude is capped by the coefficient of rolling friction μ_r (Fig.S6 d)

In this study, a link contact model is developed that implements the two kinematic constraints imposed by the links. The elongation constraint is implemented by assuming the link is a linear elastic spring capable of transmitting tensile forces. This linear spring is assigned a small nominal stiffness value of k_{nt1} when the gap between the particles is less or equal to the elongation length l_0 and is assigned a large stiffness value of k_{nt2} whenever the gap between the connected beads is greater than l_0 (Fig.S6e). This stiff spring effectively acts as a penalty, enabling tensile force to develop with minimum further deformation. The incremental tensile force developed in the spring is given by equation 15:

$$\delta F_{link} = K_{nti} \cdot \delta gap \quad [15]$$

The angular constraint is implemented by assuming a constant angular stiffness k_θ. From the position vectors of three consecutive particles connected by links in a chain: $\vec{x_0}$, $\vec{x_1}$, and $\vec{x_2}$ (Fig.S6f), two branch vectors $\vec{r_1}$ and $\vec{r_2}$ are calculated from the vector subtraction by equations 16 & 17:

$$\vec{r_1} = \vec{x_1} - \vec{x_0} \quad [16]$$

$$\vec{r_2} = \vec{x_2} - \vec{x_0} \quad [17]$$

The angle between the links (θ) is calculated from the two branch vectors as:

$$cos(\theta) = \frac{\vec{r_1} \cdot \vec{r_2}}{|\vec{r_1}||\vec{r_2}|} \quad [18]$$

Furthermore, two unit vectors $\hat{v}_1$ and $\hat{v}_1$, which lie in the plane of the branch vectors $\vec{r_1}$ and $\vec{r_2}$,(Fig.S6f) and are perpendicular to the branch vectors in the direction of increasing flex angle θ are obtained by equations 19 and 20:

$$\hat{v}_1 = \frac{(\vec{r_1} \times \vec{r_2}) \times \vec{r_1}}{|(\vec{r_1} \times \vec{r_2}) \times \vec{r_1}|} \quad [19]$$

$$\hat{v}_2 = \frac{(\vec{r_2} \times \vec{r_1}) \times \vec{r_2}}{|(\vec{r_2} \times \vec{r_1}) \times \vec{r_2}|} \quad [20]$$

If the bending angle between two links (branch vectors) becomes smaller than flex angle θ_0, then from the incremental angle change $\Delta\theta$, a scalar force magnitude Δf is computed by equations 21 and 22 :

$$\Delta\theta = \theta_0 - \theta \quad [21]$$

$$\Delta f = k_\theta \cdot \Delta\theta \quad [22]$$

In order to conserve angular momentum while applying the forces generated by the link contact, the scalar force Δf is divided into two force vectors $\Delta\vec{f}_1$ and $\Delta\vec{f}_2$ given by equations 23 & 24 respectively. The force vectors $\Delta\vec{f}_1$ and $\Delta\vec{f}_2$ are applied at the centres of the particles given by position vectors $\vec{x_1}$ and $\vec{x_2}$ such that the net moment applied by $\Delta\vec{f}_1$ and $\Delta\vec{f}_2$ is zero and both forces act in the direction of increasing bending angle θ. To conserve linear momentum, a force vector $\Delta\vec{f}_0$ is applied to the central particle (position $\vec{x_0}$), whose magnitude is equal to the vector sum of $\Delta\vec{f}_1$ and $\Delta\vec{f}_2$ (equation 25) but which acts in the opposite direction to the vector sum so that the net force applied on the three-particle system is zero.

$$\Delta\vec{f}_1 = \frac{\Delta f r_2}{r_1 + r_2} \hat{v}_1 \quad [23]$$

$$\Delta \vec{f_2} = \frac{\Delta f r_1}{r_1 + r_2} \hat{v}_2 \quad [24]$$

$$\Delta \vec{f_0} = -(\Delta \vec{f_1} + \Delta \vec{f_2}) \quad [25]$$

The values of the normal k_n and shear k_s stiffnesses in the frictional contact model were calibrated by conducting a series of simulations with varying stiffness values to strike a balance between avoiding unrealistic overlaps between the contacting particles and achieving practical simulation duration. However, the angle of repose is not sensitive to the normal and shear stiffness values as long as the overlap between the particles is not large. We obtain a stiffness value of 1e6 N/m by limiting the overlap to smaller than 0.1% of the particle radius . The normal and damping shear coefficients are assigned a value of 0.2, which is obtained from the reported coefficient of restitution of the particle material(steel)

The next series of simulations are performed to calibrate the values of the sliding and the rolling friction coefficients. The steel beads modelled in this study were obtained by cutting the links in industrially manufactured chains and isolating the individual beads. These beads have many morphological characteristics that separate them from perfectly spherical and mono-sized bead ensembles. The original shape of the steel beads is ellipsoidal, and the presence of the cavity transforms the shape into a hollow drum-like. The drum-shaped particle also has two sharp edges, thus having flat faces on the two ends. These shape characteristics increase the eccentricity of the contact normal directions for these particles, therefore, resulting in the larger angle of repose values for single bead ensembles. But for chains, the connecting links are present between the beads, therefore, the effects of particle shape are absent. Because of shape effects present in single-bead ensembles, the value of friction coefficients are calibrated separately for single-bead ensembles($M = 1$) and for chain ensembles($M = 4,12,24$). For simplicity, the values of both friction coefficients are assumed to be equal

References

1. PS Sarate, TG Murthy, P Sharma, Column to pile transition in quasi-static deposition of granular chains. *Soft Matter* **18**, 2054–2059 (2022).
2. LN Zou, X Cheng, ML Rivers, HM Jaeger, SR Nagel, The packing of granular polymer chains. *Science* **326**, 408–410 (2009).